

Contents lists available at ScienceDirect

Carbohydrate Polymer Technologies and Applications

journal homepage: www.elsevier.com/locate/carpta



Cellulose-based hydrogel beads: Preparation and characterization



Guangjun Nie^{a,*}, Yipeng Zang^a, Wenjin Yue^a, Mengmeng Wang^a, Aravind Baride^b, Aliza Sigdel^c, Srinivas Janaswamy^{c,*}

- ^a College of Biochemical Engineering, Anhui polytechnic University, 241000 Wuhu, China
- ^b Department of Chemistry, University of South Dakota, Vermillion, SD 57069, USA
- ^c Department of Dairy and Food Science, South Dakota State University, Brookings, SD 57007, USA

ARTICLE INFO

Keywords: Cellulose Beads Dissolution Zinc chloride Calcium chloride

ABSTRACT

Biopolymer-based hydrogel beads possessing intrinsic low-toxicity, biocompatibility and biodegradability have gained widespread utility in several applications. Among the biopolymers, cellulose is one of the most abundant renewable biomaterials. Herein cellulose hydrogel beads have been prepared by dissolving cellulose in 68% ZnCl₂ solution and then crosslinking the polymer chains through calcium ions. The water and ethanol washing of the beads profoundly influences the beads architecture as characterized by Fourier transform infrared spectroscopy, Raman spectroscopy, X-ray powder diffraction and Scanning electron microscopy. The total crystallinity index of the beads increases with the amount of calcium ions that is further enhanced by water washing. These beads, possessing a layer-like nanoporous structure, are capable of loading bovine serum albumin (BSA) and releasing in a sustained manner. The outcome promises a large-scale production of cellulose beads having the potential to be eco-friendly and inexpensive delivery carriers in food, pharmaceutical, medical and agriculture applications.

1. Introduction

Hydrogel beads are commonly composed of three-dimensional hydrophilic polymer networks formed through covalent bonds, hydrogen bonds and/or physical entanglements (Kato & Gehrke, 2004). They have excellent water solubility and biocompatibility, and thus find applications in drug delivery, tissue engineering and bio-adsorbents (Agarwal et al., 2015; Facciorusso, Di Maso & Muscatiello, 2016; Trivedi et al., 2018; Zhou, Fu, Zhang, Zhan & Levit, 2014). Some wellknown examples are polyethylene glycol (PEG), polyacrylamide (PAM) and polyvinyl alcohol (PVA), all hydrophilic. Their intrinsic toxicity (Dao, Cameron & Saito, 2016), however, has resisted wholesome utilization. As a result, biopolymers such as chitosan, alginate and cellulose (Gericke, Trygg & Fardim, 2013; Kim, Kim, Choi, Kimura & Wada, 2017; Ren et al., 2016; Ruan, Stromme & Lindh, 2018; Wang et al., 2013) have been examined as alternatives to create more consumer friendly hydrogels exhibiting biocompatibility, biodegradability and low-toxicity. Among them, cellulose is abundant in supply with a biosynthesis production of 10¹¹–10¹² tons/year (Sun, Sun, Zhao & Sun, 2004). It further forms the natural carbon cycle that could be easily reused through the decay process of decomposers (Gupta, Carrott, Singh, Chaudhary & Kushwaha, 2016). Consequently, native cellulose and its derivatives have gained momentum as ideal support materials for hydrogels, polymer blends, crosslinkers, rapid adsorbent materials (He et al., 2014; Guo et al., 2021; Kim et al., 2017; Ma et al., 2014; Zhang et al., 2018), drug-loaded hydrogels (Supramaniam, Adnan, Kaus & Bushra, 2018; Yang & Wang, 2018) and affinity purification beads (Shao, Xiu, Zhang, Huang & Gong, 2018), to name a few. In the case of beads, several successful protocols have been developed for preparing the cellulose beads (Gericke et al., 2013). Dissolving cellulose in NaOH-urea-water coupled with coagulation into nitric acid and saline solution is found to control beads structure (Trygg, Fardim, Gericke, Makila & Salonen, 2013). In addition, solubilizing in ionic liquids, e.g. waste denim, results in beads with nanopores having propensity to load and control release drug molecules (Zeng, Wang & Byrne, 2020). Cellulose beads with nanoporous structure have also been prepared by precipitating cellulose/LiCl/DMAc solutions into ethanol and water, and beads drying from water or ethanol is found to determine the nature of the final bead network structure (Li et al., 2020). Interestingly, incorporation of carboxymethyl cellulose (CMC) into the cellulose matrix improves water mobility and bead porosity (De Wever et al., 2021).

Despite these successful examples and considerable progress achieved by circumventing the difficulties, cellulose insolubility in water is still a major hurdle to the cellulose hydrogel proposition. Molecular details of this biopolymer at the atomic level could be helpful to find possible answers. Chemically, cellulose is a linear polysaccharide composed of β -1-4-linked D-glucopyranosyl units. The ribbon-

E-mail addresses: n.g.jason@163.com (G. Nie), Srinivas.Janaswamy@sdstate.edu (S. Janaswamy).

 $^{^{\}scriptsize{$^{\scriptsize{$^{\circ}}$}}}$ Submitted to Carbohydrate Polymer Technologies and Applications December 24, 2020.

^{*} Corresponding authors.

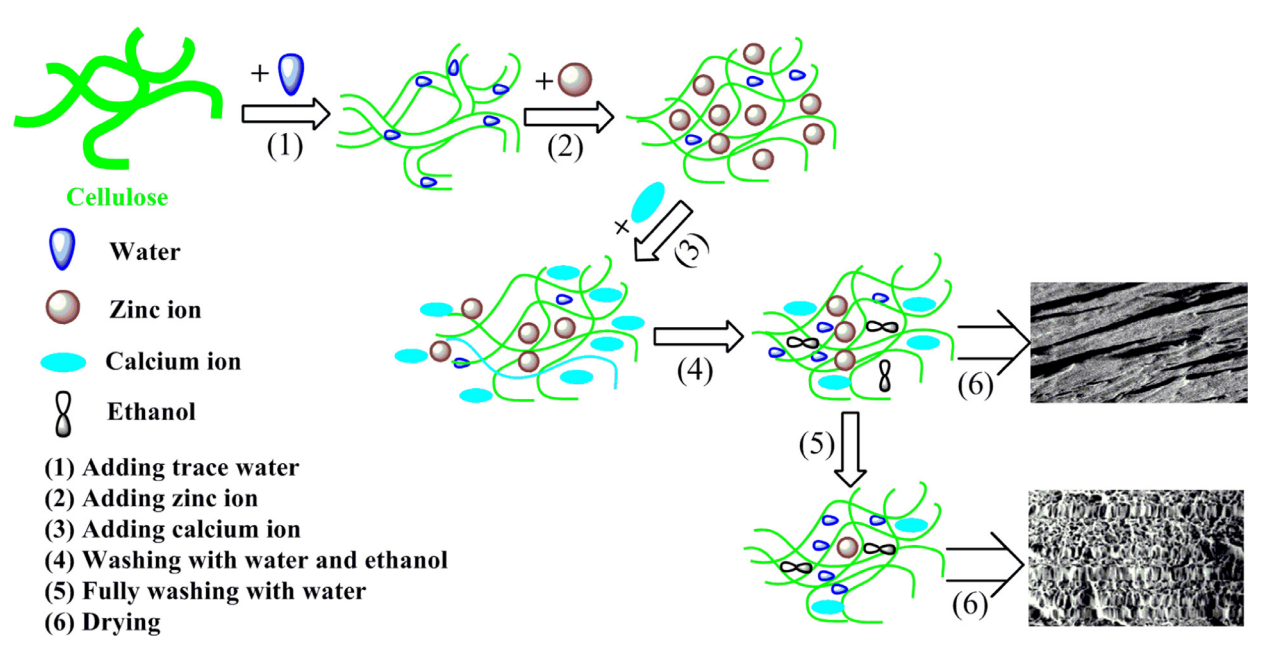


Fig. 1. Schematic representation of cellulose solubilization by zinc ions and crosslinking by calcium ions toward hydrogel beads formation. Subsequent beads washing with water and ethanol results in altered network structure in the beads.

like polysaccharide chains exist in a tight network structure stabilized by strong intra- and inter-chain hydrogen bonds (Nishiyama, Langan & Chanzy, 2002), is the self-association property that prohibits cellulose from dissolving in water (Medronho & Lindman, 2015). Many chemical methods including cellulose modification (Akalin & Pulat, 2018; Suenaga & Osada, 2018), crosslinker intrusion (Li et al., 2018; Prochon, Marzec & Szadkowski, 2019) and use of complicated solvent systems (Isobe, Kimura, Wada & Deguchi, 2018) have been explored as useful strategies to overcome this difficulty. However, shortcomings related to toxicity, environmental threat, higher power consumption and complicated solvent recovery procedures far from green protocols have limited their utility to a minimum. On the other hand, our discovery of dissolving in ZnCl2 solution (Xu, Chen, Rosswurm, Yao & Janaswamy, 2016) stands out as a promising, green and sustainable tool to solubilize cellulose. In this approach, Zn²⁺ ions are brought in for competitive binding to O3H atoms of cellulose chains by breaking the canonical O3H ••• O5 hydrogen bonds. This process disrupts the self-association of cellulose network to such an extent that effectively promotes cellulose solubility in water. The solubilized cellulose chains could then be crosslinked with calcium ions, from which high tensile strength films prepared (Xu et al., 2016). Based on this success, herein, we hypothesize that solubilized cellulose chains, crosslinked through calcium ions, could be transformed to hydrogel beads and these beads could further serve as delivery carriers of potential molecules of interest. Toward this end, in this submission, we demonstrate the preparation of cellulose hydrogel beads by first dissolving cellulose in ZnCl₂ solution and then constructing beads via crosslinking the cellulose chains with calcium ions. The effective roles of water and ethanol washing on the beads morphology has been established. In addition, beads capacity to load and release bovine serum albumin (BSA) has been demonstrated.

2. Experimental

2.1. Materials

Microcrystalline cellulose avicel PH 101 (MW = 162) was a gift from the FMC Corporation, USA. Salts $CaCl_2$ and $ZnCl_2$ and ethanol were purchased from the Fisher Scientific and were used as received along with the distilled water.

2.2. Effect of water on cellulose dissolution

It has been established that 68% ZnCl $_2$ is suitable to dissolve cellulose (Xu et al., 2016). Herein, to investigate the effect of water on cellulose dissolution, three different protocols were studied: (1) 1.6 mL distilled water was supplied into 0.8 g avicel powder after adding ZnCl $_2$ solution (16.24 g ZnCl $_2$ in 6.0 mL distilled water); (2) 1.6 mL distilled water was added into 0.8 g avicel powder before supplementing the ZnCl $_2$ solution, and (3) ZnCl $_2$ solution was added in 0.8 g avicel powder without water addition. The degree of cellulose dissolution was observed.

2.3. Cellulose gel and beads preparation

As illustrated in Fig. 1, cellulose paste was prepared by adding 0.8 g avicel powder to 1.6 mL distilled water, and then its dissolution in the $\rm ZnCl_2$ solution was studied. The zinc-cellulose gel (Cz) was obtained by mixing the solution at 65 °C (± 1) for 30 min. Duplicate Cz samples were washed, at the ambient temperature, with triple volume of distilled water and later with anhydrous ethanol for three times. The samples were referred as Czw and Cze, for brevity, in the rest of the discussion.

The hot Cz gel was added dropwise into 70% (w/v) $CaCl_2$ solution, at ambient temperature, and left for 2 hr. The resulting cellulose beads (CB) were then washed with triple volume of distilled water for 20 min for three times and air dried, and were referred as CBw. In a separate experiment, CBw beads were washed with anhydrous ethanol for 20 min for three times and air dried and named as CBew.

2.4. Calcium effect

In order to understand the role of calcium ions on the beads formation the hot Cz gel was added dropwise, as in the protocol of CB preparation, into triple volume of 0–80% (w/v) CaCl $_2$ solution. The beads were left in the solution for 2 h with mild stirring at ambient temperature.

2.5. FTIR spectroscopy and X-ray diffraction (XRD)

The FTIR spectra of beads were recorded at a resolution of 4 $\rm cm^{-1}$ in the range 400–4000 $\rm cm^{-1}$ using the Nicolet 380 FTIR Spectrometer from

the Thermo Fisher Scientific. The crystalline nature of the beads was analyzed following the wide-angle X-ray diffraction methodology using the Smartlab XRD instrument (Rigaku, Japan) with a scan speed of $2^\circ/\text{min}$ in the 2θ rage $10\text{--}40^\circ$ and a step width of 0.02° . CuKa ($\lambda=1.5418$ Å) radiation was used and the tube was operated at 40 kV and 40 mA. In order to calculate the crystallinity, in each diffraction pattern around 980 data points in the nonpeak regions were selected as background intensities from a total of 1500 data points, based on the published protocol (Hickman, Janaswamy & Yao, 2009). A sixth order polynomial was fitted using the OriginPro 2018 SR1 and the coefficients were used to estimate the background intensity at each diffraction angle using Microsoft Excel. The background profile was then scaled such that it abuts the semi-crystalline pattern. The percentage of crystallinity was calculated as follows:% crystallinity = (total area - background profile area) \times 100 / total area.

2.6. Raman spectroscopy

The Raman spectra of CBew samples were collected using the Raman spectrometer from HORIBA Scientific with a green laser 532 nm operated at a power of 10 mW. The spectra were recorded in the range $3324-3331~{\rm cm}^{-1}$ at a resolution of $1~{\rm cm}^{-1}$. For each sample, 10 scans were collected and average spectrum was reported.

2.7. Scanning electron microscopy (SEM)

Scanning electron micrographs were acquired using a Field Emission Scanning Electron Microscope (Zeiss SIGMA, 30 kV) mounted with a Schottky Field Emission filament. The cellulose beads were cut into 2–3 pieces using a spatula to expose the inside feature of the bead. One piece was mounted on a stub using an adhesive carbon tape such that the newly exposed surface is on the top. It was sputter coated with gold (Denton Desk V) to a thickness of approximately 15 nm. Images were acquired from the exposed surface using an acceleration voltage of 3 kV and the secondary electron signal was captured with an Everhart-Thornley detector.

2.8. Absorption and release of bovine serum albumin (BSA)

To understand the absorptive capacity (AC) of the cellulose beads, 0.3 g of CBew beads were immersed in 20 mL of 0.5–3.0 mg/mL BSA solution for 40 h and quantified by assaying the BSA residue. The AC and the relative absorption coefficient (R_a) were calculated using the Eqs. (1) and (2).

$$AC = \frac{\left(C_c - C_t\right)V}{m} \tag{1}$$

$$R_a = \frac{A_C \times C_{0.5}}{A_{0.5} \times C} \times 100\% \tag{2}$$

Wherein, C_0 and C_t are the original and residual concentration of BSA solution (mg/mL), and V and m are the BSA volume (mL) and CBew mass (mg). The A_c and $A_{0.5}$ are the absorption capacities of CBew at a specific concentration (C) and 0.5 mg/mL ($C_{0.5}$) of BSA solution.

In order to measure the release nature of the encapsulated BSA, initially 300 mg of CBew beads were immersed in 20 mL of 300 mg/mL BSA solution for 40 h. Later, beads were taken out and washed with distilled water, and BSA release was measured by immersing the beads in 20 mL distilled water. The concentration testing was carried out using a UV/Vis spectrophotometer. Initially, wavelength scan was performed in the range 200–500 nm for determining the optimum wavelength of absorbance of 280 nm for the BSA. Subsequently, calibration curve was generated by dissolving known amounts of BSA in distilled water. The release from the beads was measured at 1, 3, 5, 7, 10, 15, 20, 30 and 40 h and estimated using the calibration curve. Average values from triplicate measurements are reported.



Fig. 2. Enhancement of cellulose dissolution in $ZnCl_2$ solvent by water (a) adding solvent first to avicel powder and then water, (b) adding water first and solvent next, and (c) adding solvent only.

3. Results and discussion

3.1. Effect of water on cellulose dissolution

Previously, it has been established that avicel (commercial cellulose) could be dissolved in 68% ZnCl₂ (Xu et al., 2016). However, in order to understand the role of water on the cellulose dissolution, herein, three distinct experiments have been carried out; in the first two cases water is explicitly added but in the third case water is not an additive. The three panels in Fig. 2 illustrate the observations. The cellulose ZnCl2 solution, free of additional water is cloudy (Fig. 2c) but becomes less cloudy upon adding water (Fig. 2a). On the other hand, if cellulose is treated with water first and then mixed with the ZnCl2 solution, there is significant increase in solubility, yielding a transparent and homogeneous solution as clearly seen in Fig. 2b. These differences could be understood in terms of changes taking place in the molecular structure and associative properties of the cellulose chains under the influence of the solvent and cations. Cellulose chains, as in the native network structure of avicel, are stabilized by O3H ••• O5 hydrogen bonds and held together through inter-chain interactions O3H ••• O6 and O2H ••• O6 (Nishiyama et al., 2002). Such a strong hydrogen bonding network results in water insolubility. Adding water to cellulose first, however, causes the cellulose network to swell. If ZnCl₂ is added at this stage, the Zn²⁺ ions could permeate into the network and pair with the O3H atoms of the glucose units via O3H•••Zn²⁺ interactions. This in-turn will destroy the canonical O3H•••O5 hydrogen bonds thereby disturbing the cellulose network, and pave the way for eventual solubility (Figs. 1 and 2). Overall inference is that addition of water to cellulose particles is critical for the complete dissolution of cellulose chains in the ZnCl₂ solution.

3.2. Effect of calcium on the formation of beads

In order to understand the role of calcium ions on the retention of beads, the CBew beads were prepared with 0, 18, 35, 58, 70 and $80\,\mathrm{g}/100\,\mathrm{mL}\,\mathrm{CaCl_2}$ concentration. The observation was that as the CaCl₂ concentration increases, beads turn out to be whiter and harder. It has been reported that upon dissolving the cellulose in the ZnCl₂ solution, the polymer chains could be crosslinked via calcium ions (Xu et al., 2016). Thus, it appears that the presence of more calcium ions in the solution the more synergistic interactions will be among the dissolved cellulose chains, which results in harder beads.

X-ray powder diffraction analysis was carried out to follow the structural changes taking place in the CBew beads. As highlighted in Fig. 3a, avicel has three peaks at 16.4, 22.5 and 34.5° of 2θ having Miller in-

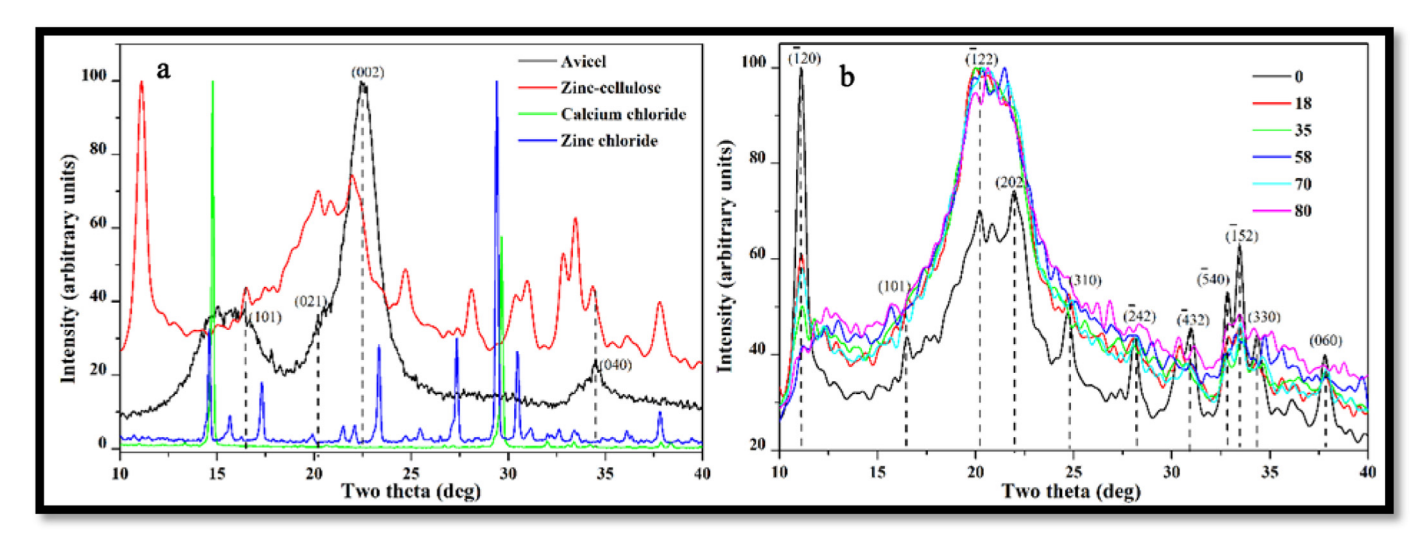


Fig. 3. (a) Comparison of X-ray powder diffraction patterns of avicel, zinc-cellulose, calcium chloride and zinc chloride (from top to bottom) and (b) CBew samples calcified by 0, 18, 35, 58, 70 and 80 g/100 mL of CaCl₂ (from top to bottom).

 $\begin{tabular}{ll} \textbf{Table 1a} \\ \textbf{Relative intensity}, \textbf{d-spacing}, \textbf{Miller indices and observed and calculated Bragg angles in the diffractogram of Zn-Cellulose}. \end{tabular}$

	Relative	0 .				2θ (°)		
Peak	intensity	d (Å)	h	k	1	Observed	Calculated	
1	100.0	7.9714	-1	2	0	11.099	11.101	
2	2.7	4.9439	0	1	2	17.941	17.931	
3	13.5	4.3960	-1	2	2	20.200	20.194	
4	8.0	4.2586	-3	3	0	20.860	20.856	
5	31.2	4.0474	2	0	2	21.960	21.988	
6	18.7	3.6041	3	1	0	24.701	24.696	
7	18.9	3.1753	-2	4	2	28.102	28.076	
8	5.3	2.9404	-4	2	2	30.399	30.422	
9	25.1	2.8865	-4	3	2	30.980	30.980	
10	17.7	2.7250	-5	4	0	32.840	32.841	
11	40.6	2.6780	-1	5	2	33.460	33.471	
12	14.7	2.6099	3	3	0	34.360	34.355	
13	1.9	2.5369	-4	6	0	35.381	35.393	
14	6.6	2.4865	-5	3	2	36.122	36.100	
15	22.9	2.3799	0	6	0	37.801	37.815	

dices (101), (002) and (040), respectively (Luengnaruemitchai & Anupapwisetkul, 2019). There is also a shoulder peak at 20° from the (021) planes. The calculated crystallinity is 37.7%. Interestingly, in the case of Cz, avicel dissolved in ZnCl₂ solution, as many as 15 peaks, sharper and crystalline, are seen at 11.1, 17.9, 20.2, 20.8, 21.9, 24.7, 28.1, 30.4, 30.9, 32.8, 33.5, 34.5, 35.4, 36.1 and 37.8° of 2θ . These new peaks clearly suggest that Zn-cellulose adopts a novel molecular structure. The calculated crystallinity is 24.5%. These peaks could be indexed on a monoclinic unit cell with the DICVOL91 program (Boultif & Louer, 2004) in the Expo-suite (Altomare et al., 2020). The unitcell dimensions are a = 14.152(5), b = 16.047(6), c = 10.541(3)Å and $\gamma = 117.21(3)^{\circ}$. The estimated figure of merit values M₁₅ (de Wolff, 1968) and F₁₅ (Smith & Snyder, 1979) are 10.4 and 12.4, respectively. Table 1a lists the relative intensity, d-spacing, Miller indices, and observed and calculated Bragg angles for all these peaks. Table 1b summarizes the unit cell dimensions of several cellulose allomorphs for comparison. Generally, cellulose molecule adapts a stiff 2-fold helical structure with a pitch of 10.4 Å that is stabilized by strong intra-chain O3H ••• O5 hydrogen bonds (Fig. 4a). Interestingly, the two branched bacterial polysaccharides xanthan and acetan have backbones the same as in cellulose, and contain trisaccharide and pentasaccharide side groups, respectively, attached to the O3H atom on alternate glucose units. As a result, it is no longer possible to form the crucial intra-chain O3H ••• O5 hydrogen bonds required for a cellulose-like molecular structure. Consequently, the backbone achieves more conformational freedom than cellulose, and novel 5-fold molecular structures are formed (Chandrasekaran & Radha, 1997; Chandrasekaran, Janaswamy & Morris, 2003) that are able to promote water solubility. Similar structural changes should be taking place in Zn-cellulose also for stabilizing its novel molecular structure (Fig. 4b). However, the observed *c*-axis value of 10.541(3) Å is similar to that of cellulose allomorphs. Interestingly, there are changes in basal net dimensions indicating that the intermolecular interactions should be very different due to Zn²⁺ ions binding to the cellulose chains. In the case of cellulose $I\beta$, two parallel cellulose chains are packed in an oblique net with a basal net area of 63.5Å². More or less similar area of 64.5 Å² is needed to accommodate the antiparallel cellulose chains in cellulose II that results due to mercerization. The same is the case (64.7 Å²) for cellulose IV due to hydrothermal treatments. Cellulose II at higher relative humidity (93%) demands a increased net area of 78.1 Å² to accommodate water molecules in the network. On the other hand, cellulose $I\alpha$ and III_1 manage with a smaller basal net area of 32.0 and 33.7 Å², respectively, in which the packing stabilizes through one equivalent cellulose chain structure. In the case of Zn-cellulose, around 101 Å² is needed to stabilize the packing modified by zinc ions and water molecules (Fig. 4b). Such a network structure could readily accommodate calcium ions crosslinked to the solubilized cellulose chains (Fig. 4c) providing additional strength to the beads. It is not clear how many cations, water molecules and cellulose chains are packed in the unit cell and thus three-dimensional structural analysis is needed to unravel the structural details.

The sharp diffraction peaks observed in Zn-cellulose continue to exist when calcium ions are also present but with reduced intensity, and could be indexed based on the Zn-cellulose unit cell values. The CBew has a few wider and higher intensity peaks at around 22° , as in regenerated cellulose II (Reddy & Yang, 2009) but without any peak at 16° (Fig. 3b). The crystallinity is 20.9, 21.4, 17.8, 20.8 and 18.5% for 18, 35, 58, 70 and 80 g/100 mL of CaCl $_2$, respectively. It was suggested that the solubility of cellulose in ZnCl $_2$ solution could be affected by the transformation of cellulose II from native cellulose I because of calcium ions. The 11° peak intensity exists up to 70% of CaCl $_2$ concentration but is less intense at 80% of CaCl $_2$. The differences in X-ray data clearly indicate that structural changes are taking place among the molecular components of the complexes (Fig. 4b and c). Further research is needed to gain a fuller picture.

Table 1bUnit cell parameters of cellulose in different allomorphs.

	Unit cell dimensions (Å, °)					Volume (ų)	Reference	
Type	a	b	с	α	β	γ		
Ια	6.72	5.96	10.40	118.1	114.8	80.4	333.3	Nishiyama, Sugiyama, Chanzy & Langan, 2003
Iβ	7.78	8.20	10.38	90	90	95.5	659.6	Nishiyama et al., 2002
II	8.01	9.04	10.36	90	90	117.1	667.8	Langan, Nishiyama & Chanzy, 1999
II-hydrate	9.02	9.63	10.34	90	90	116.0	807.3	Lee & Blackwell, 1981
III ₁	4.45	7.85	10.31	90	90	105.1	347.7	Wada, Chanzy, Nishiyama & Langan, 2004
IV ₁	8.03	8.13	10.34	90	90	90	675.0	Gardiner & Sarko, 1985
IV ₂	7.99	8.10	10.34	90	90	90	669.2	Gardiner & Sarko, 1985
Zn-Cellulose	14.152(5)	16.047(6)	10.541(3)	90	90	117.21(3)	1064.5	Present work

 Table 2

 Effect of calcium concentration on the CBew crystallization.

Calcium concentration/%	A _{cr}	A _{Ca}	CD _{Ca} /%	FWHM of 481 cm ⁻¹
0	3231.17	1.1632	0.04	12.61
18	2897.97	5.1776	0.18	14.78
58	3397.52	6.4371	0.19	14.91
70	3166.29	11.2396	0.35	16.01
80	3007.47	2.4777	0.08	14.26

The SEM images of CBew are shown in Fig. 5. The beads without calcium ions have finer pores and are uniformly distributed (Fig. 5a). However, when the calcium concentration is increased, regular pores (~50 nm) are formed, leading to an orchestrated network structure in the beads (Fig. 5b–d). Layers of nanoporous structure start to appear at around 70% of CaCl₂ concentration but at 80%, CaCl₂ begins to deposit on the beads (Fig. 5e). Thus, 70% CaCl₂ concentration appears to be optimum for preparing the cellulose beads (Fig. 5d). These observations are in agreement with the X-ray diffraction measurements.

To further understand the effect of calcium ions on the CBew beads, samples were analyzed through Raman spectroscopy. The Fig. 6a highlights the patterns in the two ranges 3200–2800 cm $^{-1}$ and 1600–300 cm $^{-1}$ that correspond to amorphous and crystalline cellulose structures, respectively (Szymańska-Chargot, Cybulska & Zdunek, 2011). The total area under the crystalline peaks was defined as the crystallization area (A_{cr}). The skeletal bending modes of CCC, COC, OCC and OCO are dominant in the 150–550 cm $^{-1}$ region and the Fig. 6b highlights characteristic peaks at 554, 527 and 481 cm $^{-1}$ that are seen only in the beads containing calcium ions, clearly suggesting the impact of calcium ions on the cellulose structure in the beads. Due to significant difference each from the corresponding part of non-calcified beads, the 481 cm $^{-1}$ peak area was chosen to be the crystallized area of calcified cellulose (A_{Ca}). The percentage of A_{Ca} to A_{cr}, which reflects the crystallinity of calcified cellulose (CD_{Ca}), is a measure of the calcium binding to cellulose chains.

The full-width-at-half-maximum (FWHM) could also signify the crystallinity. As shown in Table 2, $\rm CD_{Ca}$ is positively correlates with the FWHM at 481 $\rm cm^{-1}$. The beads prepared with the 70% $\rm CaCl_2$ solution have the highest values of FWHM and $\rm CD_{Ca}$, suggesting 70% $\rm CaCl_2$ as the optimum concentration for improving the crystallization in the CBew beads, and in agreement with X-ray and SEM observations.

3.3. FTIR characterization

The FTIR spectra of the avicel, Cz, Czw, Cze and CBw are shown in Fig. 7a. The significant peaks are zoomed in Fig. 7b–d. The wide band observed at 3100–3600 cm⁻¹ (Fig. 7b) is attributed to OH stretching from the absorbed water (Lambert, Shurvell, Lightner & Cooks, 1987). The ranges 3455–3410 cm⁻¹ and 3375–3340 cm⁻¹ correspond to the intramolecular hydrogen bonds O2H•••O6 and O3H•••O5, respectively. The 3336 cm⁻¹ band in avicel changes to 3386 cm⁻¹ in Cz. This shift

could be attributed to Zn2+ ions binding to the O3H hydroxyl groups leading to new O3H•••Zn²⁺ interactions. Furthermore, Zn²⁺ ions bridge adjacent cellulose chain, thereby increasing the number of intermolecular hydrogen bonds in Cz. Apart from the permeating Zn²⁺ ions, water molecules entering the network could also increase the lateral separation between the cellulose chains. The delicate interplay of these distinct events results in the cellulose dissolution in the ZnCl₂ solution. Similar to CBw, the band of Czw shifts back to 3336 cm⁻¹ from that of Cz. The excess-water-washing of Czw might have depleted the Zn²⁺ ions amount that could in-turn influence the number of O3H•••Zn²⁺ interactions as well as perturb the corresponding band. Compared to Czw, the FWHM of CBw is relatively smaller for 3336 cm⁻¹ suggesting the intact O3H•••O5 hydrogen bonds but with weaning of a few hydrogen-bonds. It appears that after adding calcium ions, O3H•••Zn²⁺ interactions get stabilized along with chain crosslinking and in-turn reduce the available water molecules to cellulose chains. The CBw also possess two specific bands at 3490-3440 cm⁻¹, characteristics of CaCl₂. Unlike the Cz and CBw, the Cze is more similar to the Cz pattern with a common band at 3386 cm⁻¹. Thus, it appears that ethanol was not able to remove excess Zn²⁺ ions from Cz than the water. Compared to Czw, Cze displays two tiny bands at 3208-2981 cm⁻¹, which could be due to loss of hydrogen bonds. However, presence of ethanol in the cellulose network might result in the ethanol binding to the carboxyl groups instead of water molecules, meaning an insertion of its C-C skeleton in between the cellulose chains, which might result in stiffer structure of Cze but not fragile as observed before ethanol washing.

The Fig. 7c compares the spectra in the range of $1771-1224~\rm cm^{-1}$. It is found that presence of Zn^{2+} ions shifts the bands to lower wavenumbers, in addition to reducing the transmittance. Water washing increases the transmittance but weakens the band shift. The band at $1633~\rm cm^{-1}$ is from water molecules absorbed in the cellulose (Poletto, Pistor, Zeni & Zattera, 2011; Rosa et al., 2010). Water retention decreases with the removal of Zn^{2+} ions in the beads. This could be the reason for Cze to be similar to Cz but different from Czw and CBw. Upon Zn^{2+} ions removal, the Czw and CBw beads also shirk and become stiffer.

The Fig. 7d highlights the spectra in the range of 1230–713 cm⁻¹. The bands at $1119-898~{\rm cm}^{-1}$ are noticed in avicel, Czw, CBw and Cze but not in the Cz. It indicates that these two bands could be specific to natural avicel but are lost upon Zn²⁺ ions binding to the cellulose chains in Cz. The band at 897 cm⁻¹ is assigned to the amorphous regions of cellulose (Poletto et al., 2011). Comparison of the FWHM of 898 cm⁻¹ suggests that Czw and CBw hold higher value than Cze followed by Cz, which is consistent with the presence of Zn²⁺ ions. Moreover, Zn²⁺ ions could weaken the amorphous structure of Cz but washing, particularly with water, could improve the amorphous composition by removing excess Zn²⁺ ions in the beads. This finding further reinforces that water washing is better suited to remove excess Zn²⁺ ions in the beads than the ethanol. The avicel band at 1160 cm⁻¹ downshifts to 1157 cm⁻¹ in Cz, Czw, CBw and Cze possibly due to the Zn²⁺ ions. In addition, bands at $1052-1029 \text{ cm}^{-1}$ are upshifted to 1068 and 1018 cm⁻¹ in Cz. However, upon binding to Zn2+ ions, FWHMs in Cz decrease. On the other hand,

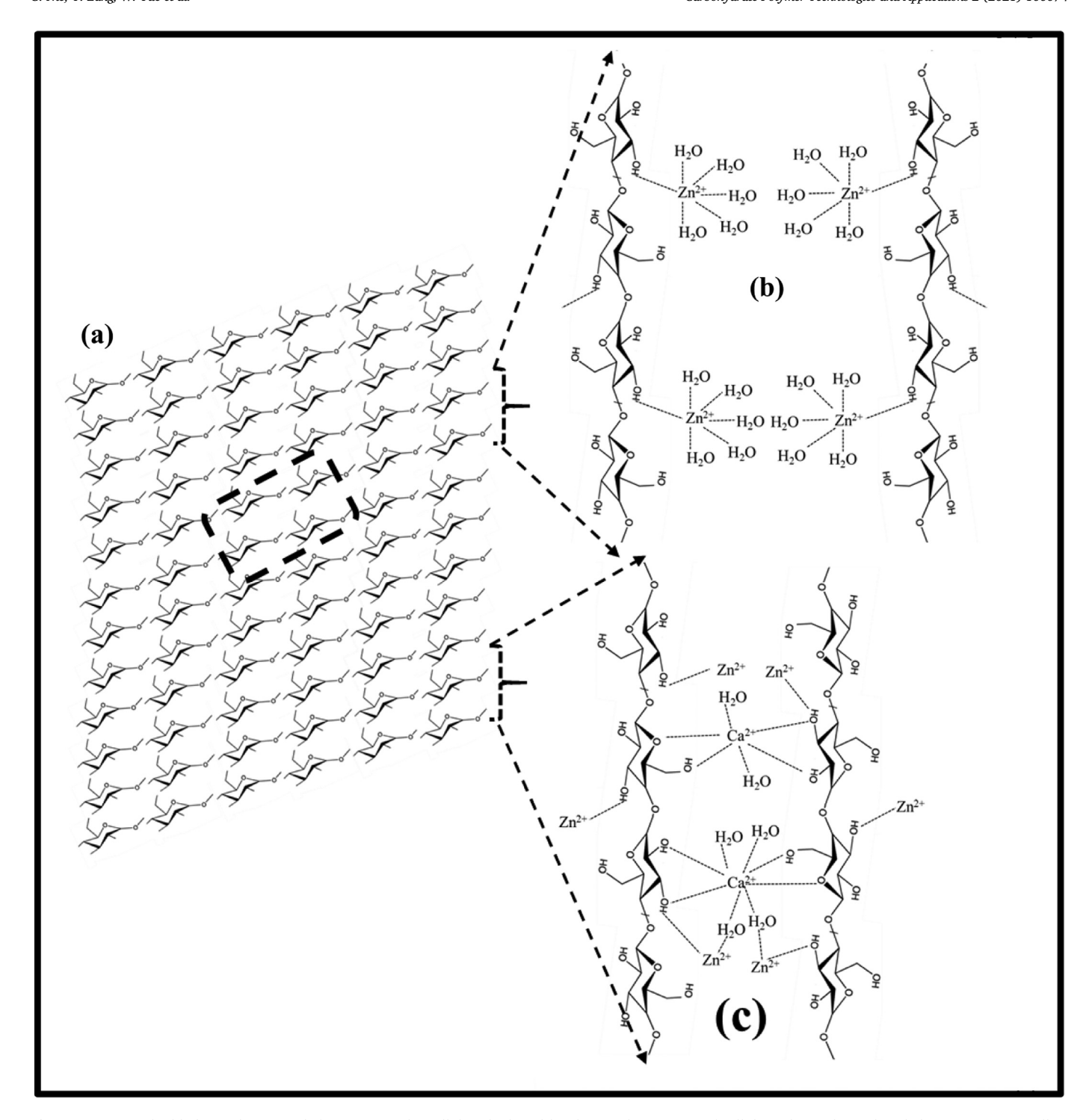


Fig. 4. A cartoon highlighting the network formation in the cellulose hydrogel beads. (a) The 12 rows of cellulose chains down their helix axes in a crystalline lattice is depicted. Hydroxyl groups and hydrogen atoms are removed, for clarity, and each glucose ring shown represents a cellulose molecule viewed down its helix axis. The unit cell (dashed rectangle) contains 4 helices. Subtle conformational changes, specific inter chain interactions and up-or-down polarity of the cellulose chains in the unit cell result in a variety of polymorphs as narrated in Table 1b, (b) when ZnCl₂ is added, the Zn²⁺ ions can break the strong O3H•••O5 hydrogen bonds by pairing with the O3H atoms; as a result, cellulose chain becomes more flexible, the crystalline network expands and lets in water molecules (H₂O) leading to cellulose solubility, and (c) further addition of calcium ions could crosslink adjacent Zn-cellulose chains resulting in more orchestrated network structure in the hydrogel beads.

in Czw, bands at $1060-1022~{\rm cm}^{-1}$ appear to approach avicel bands with increased FWHMs. These differences could be attributed to the removal of ${\rm Zn}^{2+}$ ions through water washing. Interestingly, bands at $1060-1018~{\rm cm}^{-1}$ in Czw and CBw are with reduced FWHMs relative to the Czw, which could be ascribed to the coordination of ${\rm Zn}^{2+}$ ions along with

 Ca^{2+} ions. Indeed, such an arrangement limits water role to wash away the excess $\text{Ca}^{2+}\text{and }\text{Zn}^{2+}$ ions.

The ratio of A1373 cm⁻¹/A2900 cm⁻¹ and A1430 cm⁻¹/A897 cm⁻¹ is used to assess the total crystallinity index (TCI) and lateral order index (LOI), which refer to degree of crystallinity and presence of na-

Table 3Crystallinity index of untreated and treated cellulose samples.

Sample	$A1373~cm^{-1}$	A2900 cm ⁻¹	A1430 cm ⁻¹	A897 cm ⁻¹	TCI	LOI
Avicel	0.021	0.042	0.017	0.025	0.50	0.68
Cz	0.023	0.065	0.032	0.057	0.35	0.56
Czw	0.074	0.066	0.050	0.124	1.12	0.40
Cze	0.046	0.087	0.049	0.062	0.53	0.79
CBw	0.042	0.025	0.027	0.080	1.68	0.34

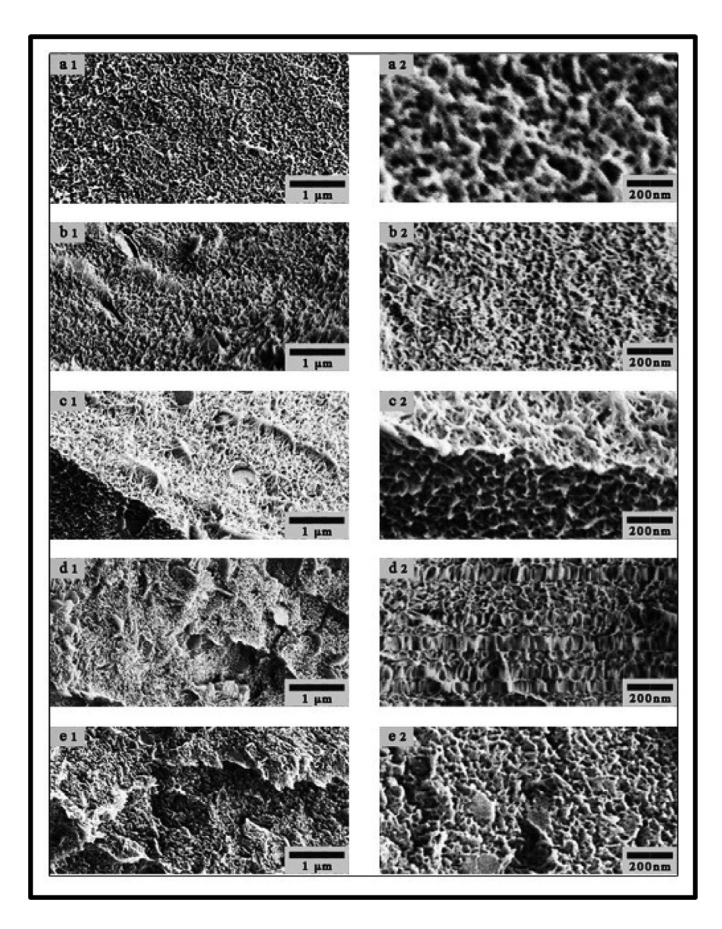


Fig. 5. The cross-section of cellulose beads in the presence of (a) 0, (b) 35, (c) 58, (d) 70 and (e) 80% of CaCl₂.

tive cellulose I in the sample, respectively. Higher TCI and LOI values correspond to higher crystallinity and natural ordered structure (Hospodarova, Singovszka & Stevulova, 2018; Luengnaruemitchai & Anupapwisetkul, 2019). The calculated TCI and LOI values of the beads are summarized in Table 3. The untreated cellulose has a TCI and LOI of 0.5–0.68, respectively, higher than the Cz. This indicates that Zn²⁺ ions result in a decreased cellulose crystallinity along with the transformation of untreated cellulose to an amorphous form. Water washing makes Czw to gain higher TCI of 1.12 but with LOI of 0.40 compared to 0.35-0.56, in the same order, of Cz, suggesting that water washing increases the cellulose crystallinity. As compared to Cz and Czw, Cze has a TCI of 0.53, close to that of avicel, but with a highest LOI of 0.79 signifying that ethanol is not suited well than water to improve cellulose crystallinity, however, it could greatly promote transformation of amorphous cellulose to crystalline cellulose. The CBw has the highest TCI of 1.68 and the lowest LOI of 0.34 signifying that calcification is highly suited to enhance the cellulose crystallinity.

3.4. Application

Since the FTIR analysis is consistent with the observation that water washing removes both zinc and calcium ions from the cellulose complexes, additional experiments using samples before and after washing were analyzed through SEM for quantifying the removal effect. In terms of physical appearance after complete water washing, which apparently removes any superfluous free zinc and calcium ions in the system, it is not surprising that CBew shrinks significantly in size. Fig. 8 highlights that CBew surface changes from a slab-like (panel a) to a nanoporous honeycomb-like structure (panel c); the corresponding vertical sections are shown in panels b and d. The porous structures would be of great importance as a carrier material for food, pharmaceutical and biomedical applications.

In order to quantify the dependence of sustained release on calcium concentration, several CBew samples were calcified using 0-80% of CaCl₂ solution and then fully washed with water in a stepwise manner. The loss in mass after final washing as a function of calcium concentration is portrayed in Fig. 9a. It suggests that initially in the calcium concentration range of 0-40% the ratio of mass loss stays low and steady at around 27%, then increases to 39% at 70% calcium and finally drops to 40% at 80% calcium concentration. Though, the residual amount does not positively correlate with the calcium concentration. the nanoporous structure obtained with 70% calcium could aid to encapsulate molecules of interest in the beads. The beads water retention capacity gradually weakens with washing time and is completely lost after 120 min of washing. This indicates that the amount of salt still remaining in the bead controls the water retention. When the residual salt is fully removed by water washing, the CBew takes up a collapsed 'empty' structure as in Fig. 8c and d that could readily serve as a delivery vehicle for functional molecules of interest.

In order to test this hypothesis, bovine serum albumin (BSA) has been used as the model compound and Fig. 9b shows that the CBew absorption increase from 5 to 200% and highly correlates with the BSA concentration range of 0.5-3 mg/mL. Unlike this linear plot, the relative adsorption coefficient Ra initially increases from 100 to 200% as BSA concentration surges from 0.4 to 1.5 mg/mL, then falls a bit, but later ascends to a maximum of 205% at 3.0 mg/mL BSA. After 40 h, the CBew beads added to 3.0 mg/mL BSA solution are able to load around 26 mg of BSA. Fig. 9c depicts the release nature of BSA from the cellulose beads. The release increases gradually and reaches saturation at around 30 h. At this time, roughly 71% of the embedded BSA has been released. The release kinetics of BSA from the cellulose beads are further analyzed by mathematical models (Costa & Lobo, 2001) using the Microsoft Excel plugin DDSolver (Zhang et al., 2010). The data were fitted with fourteen models, namely zero order, first order, Higuchi, Korsmeyer-Peppas, Hixson-Crowell, Hopfenberg, Baker-Londsale, Makoid-Banakar, Peppas-Sahlin, Quadratic, Weibull, Logistic, Gompertz and Probit. The better fitness was concluded by comparing the R square (R²) and the Akaike Information Criteria (AIC) values. The AIC is a measure of the best fit based on the maximum probability with smallest AIC value. Table 4 lists the R² and AIC values for each model fitting. It appears that the pattern of BSA release from the cellulose beads follows the first order release kinetics (highest coefficient

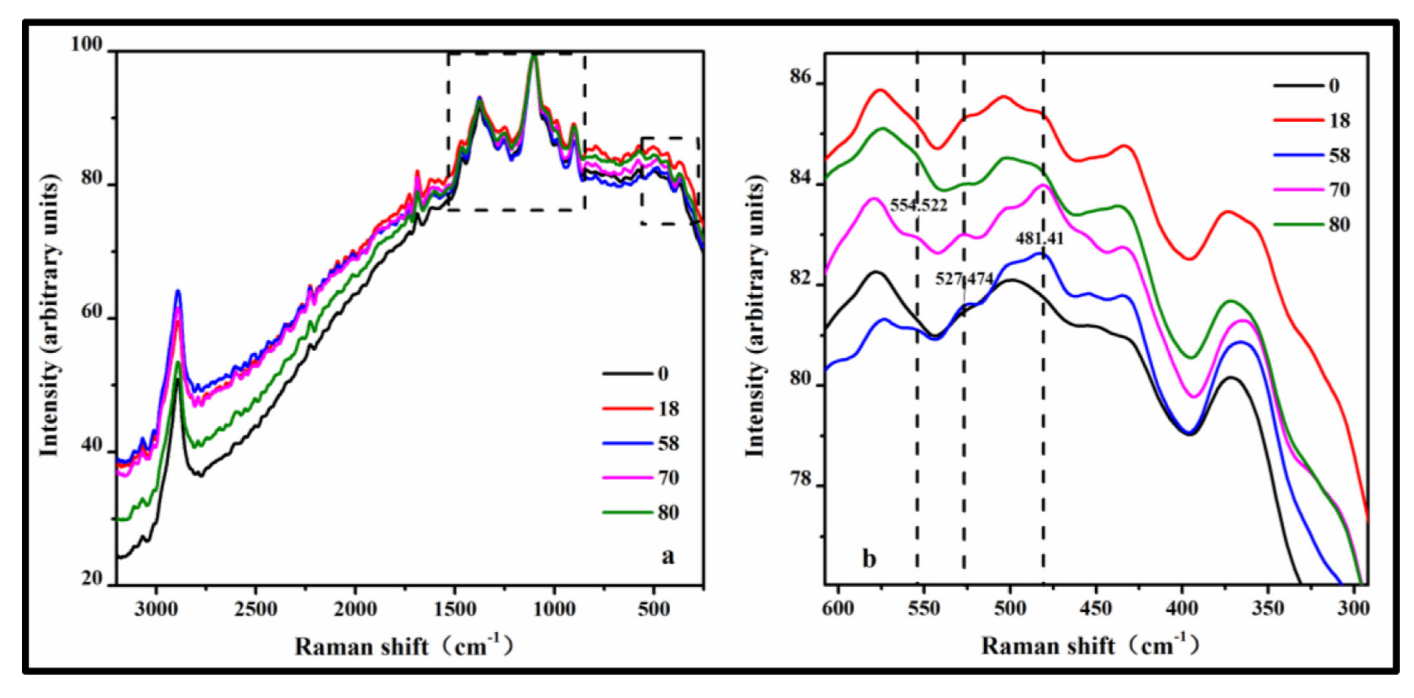


Fig. 6. Raman spectra of CBew beads: (a) whole pattern and (b) in the 600 to 300 cm⁻¹ region.

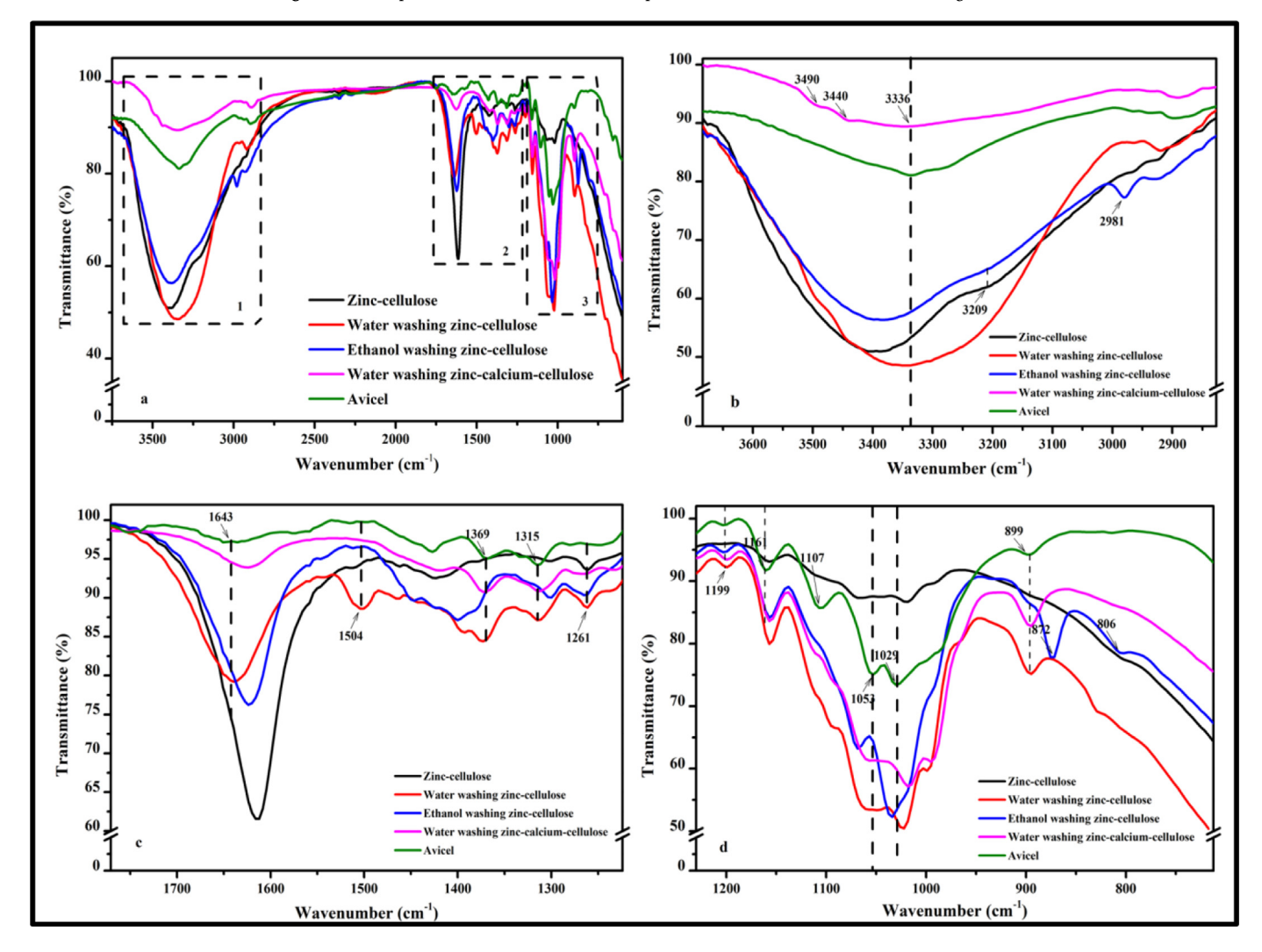


Fig. 7. Comparison of FTIR spectra of zinc-cellulose (Cz), water washed zinc-cellulose (Czw), ethanol washed zinc-cellulose (Cze), water washed zinc-cellulose (CBw), and avicel (from top to bottom) in the region (a) $4000-400 \text{ cm}^{-1}$, (b) $3683-2826 \text{ cm}^{-1}$, (c) $1771-1224 \text{ cm}^{-1}$ and (d) $1230-713 \text{ cm}^{-1}$.

Table 4 The \mathbb{R}^2 and AIC values from different mathematical models for the BSA release from the cellulose beads.

Model	Equation	R ²	AIC
Zero-order	$F=F_0+k_0*t$	0.7613	-11.7696
First-order	$F=Fmax*{1-exp[-k_1*(t-Tlag)]}$	0.9974	-46.0204
Higuchi	$F=F_0+k_H*t^0.5$	0.9101	-19.5797
Korsmeyer-Peppas	$F=F0+k_{KP}*t^n$	0.9900	-35.1891
Hixson-Crowell	$F=100*[1-(1-k_{HC}*t)^3]$	0.1396	-3.5115
Hopfenberg	$F=100*[1-(1-k_{HB}*t)^n]$	0.1415	-1.5297
Baker-Lonsdale	$3/2*[1-(1-F/100)^(2/3)]-F/100=k_{BL}*t$	0.9018	-20.8790
Makoid-Banakar	$F=k_{MB}*(t-Tlag)^n*Exp[-k*(t-Tlag)]$	0.9905	-35.5783
Peppas-Sahlin	$F=k_1*t^m+k_2*t^(2*m)$	0.9871	-33.1175
Quadratic	$F=100*(k_1*t^2+k_2*t)$	0.9040	-19.0582
Weibull	$F=100*\{1-Exp[-(t^{}\beta)/\alpha]\}$	0.9764	-28.2873
Logistic	$F=100* Exp[\alpha+\beta*\log(t)]/\{1+Exp[\alpha+\beta*\log(t)]\}$	0.9279	-21.3422
Gompertz	$F=100*Exp{-\alpha*Exp[-\beta*log(t)]}$	0.9443	-23.4171
Probit	$F=100^*\Phi[\alpha+\beta^*\log(t)]$	0.9373	-22.4680

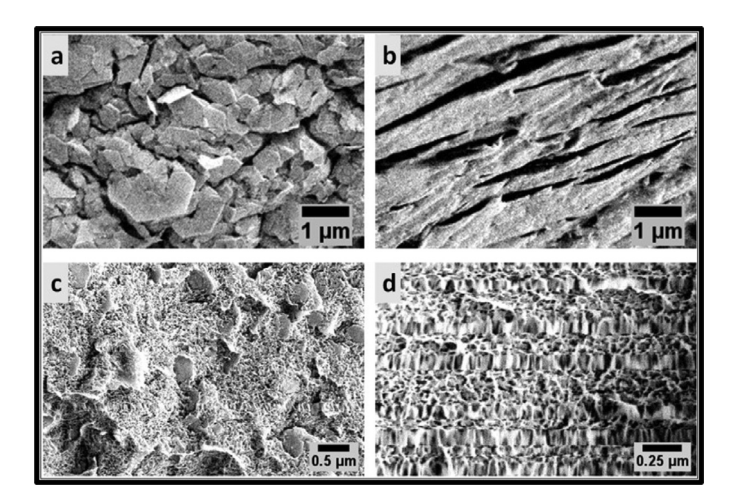


Fig. 8. SEM images of the surface (a and c) and cut (b and d) of CBew beads with 70% calcium chloride before (top) and after (bottom) water washing.

of correlation of $R^2=0.9974$ and AIC=-46.0204). In other words, release rate is directly proportional to the concentration of BSA remaining within the beads. Overall, it appears that the layer-like nanoporous network structure in the beads is key for the loading and sustained release of BSA. These beads, indeed, hold promise as delivery vehicles in several research areas.

4. Conclusions

The demand for cellulose-based products is growing due to several advantages: renewable, inexpensive and biodegradable. Herein, cellulose hydrogel beads have been prepared by first solubilizing cellulose in ZnCl₂ and then crosslinking the cellulose chains by calcium ions. The addition of calcium is responsible for obtaining the beads. Washing the beads with either water or ethanol influences their strength. While the crystallinity of beads increases as more Zn-cellulose chains are crosslinked with the calcium ions, water washing is more pronounced than ethanol washing. X-ray power diffraction analysis reveals that the Zn-cellulose complex has new, sharp and crystalline peaks, even after the calcium ions crosslink adjacent Zn-cellulose chains, while native cellulose has only broad and shallow peaks. This suggests that a novel

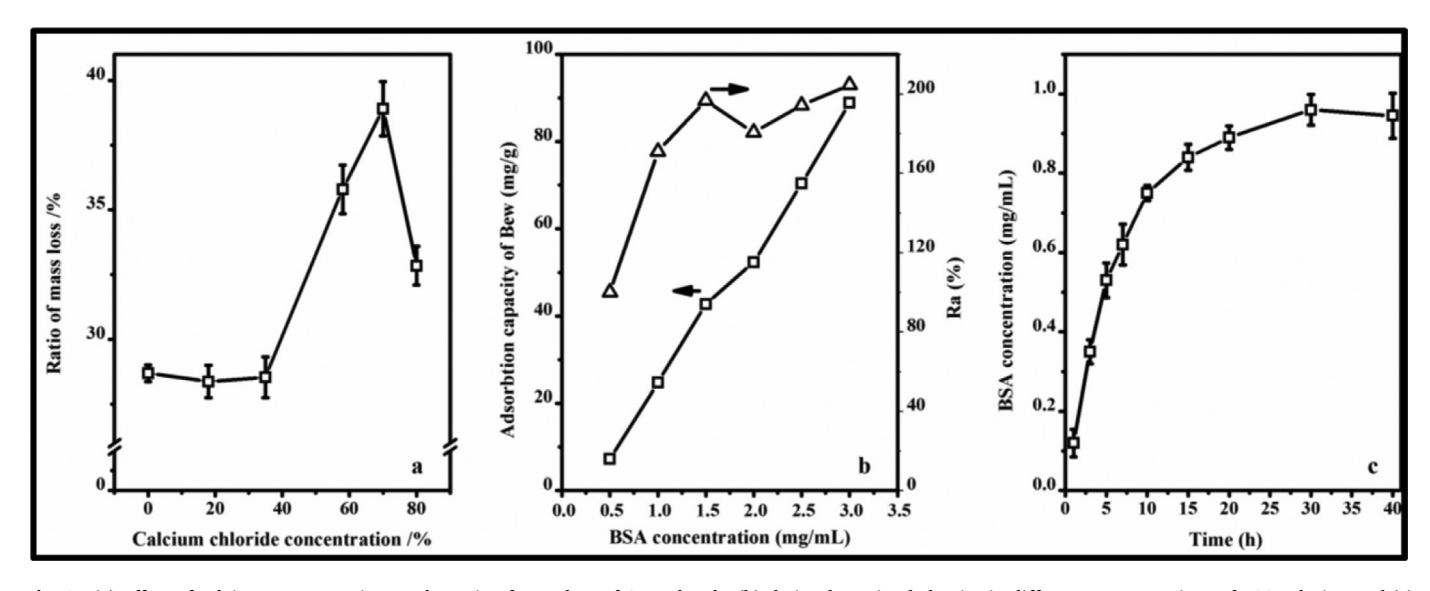


Fig. 9. (a) Effect of calcium concentration on the ratio of mass loss of CBew beads, (b) their adsorption behavior in different concentrations of BSA solution and (c) release nature of BSA from the CBew beads. The CBew were washed stepwise by three times. The first two steps are given in 'Materials and Methods'; the final step involves fully washing with distilled water until the mass is unchanged.

molecular structure exists for cellulose upon binding to Zn ions, substantially distinct from the conventional stiff ribbon structure and could be the explanation for achieving cellulose solubility in ZnCl₂. The beads possess a nanoporous layered network structure. In order to test the loading capacity of the beads, bovine serum albumin (BSA) has been used as the test bed and the results suggest around 70% of BSA loading persists even after 30 h. The beads release the encapsulated BSA in a sustained manner and follows the first order kinetics principle. Overall, cellulose hydrogel beads prepared by a two-step dissolution and twostep washing without using toxic solvents stands out as a simple and green process. It is a viable protocol to design and develop large-scale cellulose-based hydrogel beads with potential applications in biomedical (Calo & Khutoryankiy, 2015) and pharmaceutical (Peppas, Bures, Leobandung & Ichikawa, 2000) fields as well as delivery carriers of drugs (Kharkwal & Janaswamy, 2016) and nutraceuticals (Janaswamy & Youngren, 2012; Polowsky & Janaswamy, 2015).

Declaration of Competing Interest

Authors declare no conflict of interest.

Acknowledgments

Financial support is from the Studying Abroad Foundation of Anhui Polytechnic University and the USDA National Institute for Food and Agriculture (SD00H648–18, SD00G677–20, 2021–67022–33469). Thanks are to Dr. Anamika Prasad and Shengang Wang for Raman and FTIR instrument access.

References

- Agarwal, T., Narayana, S. N. G. H., Pal, K., Pramanik, K., Giri, S., & Banerjee, I. (2015). Calcium alginate-carboxymethyl cellulose beads for colon-targeted drug delivery. *International Journal of Biological Macromolecules*, 75, 409–417.
- Akalin, G. O., & Pulat, M. (2018). Preparation and characterization of nanoporous sodium carboxymethyl cellulose hydrogel beads. *Journal of Nanomaterials*, 2018, Article 9676949.
- Altomare, A., Camalli, M., Cuocci, C., Giacovazzo, C., Moliterni, A., & Rizzi, R. (2020). EXPO. A program for automatic solution and refinement of crystal structures http://www.ic.cnr.it/.
- Boultif, A., & Louer, D. (2004). Powder pattern indexing with the dichotomy method. Journal of Applied Crystallography, 37, 724–731.
- Calo, E., & Khutoryanskiy, V. V. (2015). Biomedical applications of hydrogels: A review of patents and commercial products. European Polymer Journal, 65, 252–267.
- Chandrasekaran, R., Janaswamy, S., & Morris, V. J. (2003). Acetan: Glucomannan interactions - a molecular modeling study. Carbohydrate Research, 338, 2889–2898.
- Chandrasekaran, R., & Radha, A. (1997). Molecular modeling of xanthan:gAlactomannan interactions. *Carbohydrate Polymers*, 32, 201–208.
- Costa, P., & Lobo, J. M. S. (2001). Modeling and comparison of dissolution profiles. European Journal of Pharmaceutical Sciences, 13, 123–133.
- Dao, V. H., Cameron, N. R., & Saito, K. (2016). Synthesis, properties and performance of organic polymers employed inflocculation applications. *Polymer Chemistry*, 11–25.
- De Wever, P., De Oliveira-Silva, R., Marreiros, J., Ameloot, R., Sakellariou, D., & Fardim, P. (2021). Topochemical engineering of cellulose-carboxymethyl cellulose beads: A low-filed NMR relaxometr study. *Molecules*, 26, 14.
- De Wolff, P. M. (1968). A simplified criterion for the realibility of a powder pattern indexing. *Journal of Applied Crystallography*, 1, 108–113.
- Facciorusso, A., Di Maso, M., & Muscatiello, N. (2016). Drug-eluting beads versus conventional chemoembolization for the treatment of unresectable hepatocellular carcinoma: A meta-analysis. *Digestive and Liver Disease*, 48, 571–577.
- Gardiner, E. S., & Sarko, A. (1985). Packing analysis of carbohydrates and polysaccharides. 16. The crystal structures of cellulose ${\rm IV_I}$ and ${\rm IV_{II}}$. Canadian Journal of Chemistry, 63, 173–180.
- Gericke, M., Trygg, J., & Fardim, P. (2013). Functional cellulose beads: Preparation, characterization, and applications. *Chemical Reviews*, 113, 4812–4836.
- Guo, K., Zhu, W., Wang, J., Sun, W., Zhou, S., & He, M. (2021). Fabrication of gradient anisotropic cellulose hydrogels for applications in micro-strain sensing. *Carbohydrate Polymers*, 258, Article 117694.
- Gupta, V., Carrott, P., Singh, R., Chaudhary, M., & Kushwaha, S. (2016). Cellulose: A review as natural, modified and activated carbon adsorbent. *Bioresource Technology*, 216, 1066–1076.
- He, Z., Song, H., Cui, Y., Zhu, W., Du, K., & Yao, S. (2014). Porous spherical cellulose carrier modified with polyethyleneimine and its adsorption for Cr(III) and Fe(III) from aqueous solutions. Chinese Journal of Chemical Engineering, 22, 984–990.
- Hickman, E., Janaswamy, S., & Yao, Y. (2009). Autoclave and β-amylolysis lead to reduced in vitro digestibility of starch. *Journal of Agricultural and Food Chemistry*, 57, 7005–7012.

- Hospodarova, V., Singovszka, E., & Stevulova, N. (2018). Characterization of cellulosic fibers by FTIR spectroscopy for theirfurther implementation to building materials. *American Journal of Analytical Chemistry*, 09, 303–310.
- Isobe, N., Kimura, S., Wada, M., & Deguchi, S. (2018). Poroelasticity of cellulose hydrogel. Journal of the Taiwan Institute of Chemical Engineers, 92, 118–122.
- Janaswamy, S., & Youngren, S. R. (2012). Hydrocolloid-based nutraceutical delivery systems. Food & Function, 3, 503–507.
- Kato, N., & Gehrke, S. H. (2004). Microporous, fast response cellulose ether hydrogel prepared by freeze-drying. Colloids and Surfaces B: Biointerfaces, 38, 191–196.
- Kharkwal, H., & Janaswamy, S. (2016). *Natural polymers for drug delivery*. Boston: CABI.
- Kim, U. J., Kim, H. J., Choi, J. W., Kimura, S., & Wada, M. (2017). Cellulose-chitosan beads crosslinked by dialdehyde cellulose. *Cellulose*. 24. 5517–5528.
- Lambert, J. B., Shurvell, H. F., Lightner, D. A., & Cooks, R. G. (1987). Introduction to organic spectroscopy. New York: Macmillan.
- Langan, P., Nishiyama, Y., & Chanzy, H. (1999). A revised structure and hydrogen-bonding system in cellulose II from a neutron fiber diffraction analysis. *Journal of the American Chemical Society*, 121, 9940–9946.
- Lee, D. M., & Blackwell, J. (1981). Structure of cellulose II hydrate. Biopolymers, 20, 2165–2179.
- Li, H., Kruteva, K., Mystek, K., Dulle, M., Ji, W., Petersson, T., et al. (2020). Macro- and microstructural evolution during drying of regenerated cellulose beads. ACS Nano, 14, 6774–6784.
- Li, L., Lu, F., Wang, C., Zhang, F., Liang, W., Kuga, S., et al. (2018). Flexible double-cross-linked cellulose-based hydrogel and aerogel membrane for supercapacitor separator. *Journal of Materials Chemistry A*, 6, 24468–24478.
- Luengnaruemitchai, A., & Anupapwisetkul, C. (2019). Surface morphology and cellulose structure of Napier grass pretreated with the ionic liquid 1-ethyl-3-methylimidazolium acetate combined with either water or dimethyl sulfoxide as a co-solvent under microwave irradiation. Biomass Conversion and Biorefinery, 10, 435–446.
- Ma, G., Zhang, J., Chen, L., Liu, T., Yu, L., Liu, X., et al. (2014). Amino-functionalized ordered mesoporous silica SBA-15: A rapid and efficient adsorbent for the adsorption of (-)-epigallocatechin gallate from green tea extract. RSC Advances, 4, 41341–41347.
- Medronho, B., & Lindman, B. (2015). Brief overview on cellulose dissolution/regeneration interactions and mechanisms. Advances in Colloid and Interface Science, 222, 502–508.
- Nishiyama, Y., Langan, P., & Chanzy, H. (2002). Crystal structure and hydrogen-bonding system in cellulose Iβ from synchrotron X-ray and neutron fiber diffraction. *Journal of the American Chemical Society*, 124, 9074–9082.
- Nishiyama, Y., Sugiyama, J., Chanzy, H., & Langan, P. (2003). Crystal structure and hydrogen-bonding system in cellulose $I\alpha$ from synchrotron X-ray and neutron fiber diffraction. *Journal of the American Chemical Society*, 125, 14300–14306.
- Peppas, N. A., Bures, P., Leobandung, W., & Ichikawa, H. (2000). Hydrogels in pharmaceutical formulations. European Journal of Pharmaceutics and Biopharmaceutics, 50, 27–46.
- Poletto, M., Pistor, V., Zeni, M., & Zattera, A. J. (2011). Crystalline properties and decomposition kinetics of cellulose fibers in wood pulp obtained by two pulping processes. Polymer Degradation and Stability, 96, 679–685.
- Polowsky, P. J., & Janaswamy, S. (2015). Hydrocolloid-based nutraceutical delivery systems: Effect of counter-ions on the encapsulation and release. Food Hydrocolloids, 43, 658–663.
- Prochon, M., Marzec, A., & Szadkowski, B. J. M. (2019). Preparation and characterization of new environmentally friendly starch-cellulose materials modified with casein or gelatin for agricultural applications. *Materials*, 12, 1684–1702.
- Reddy, N., & Yang, Y. (2009). Properties and potential applications of natural cellulose fibers from the bark of cotton stalks. *Bioresource Technology*, 100, 3563–3569.
- Ren, H., Gao, Z., Wu, D., Jiang, J., Sun, Y., & Luo, C. (2016). Efficient Pb(II) removal using sodium alginate-carboxymethyl cellulose gel beads: Preparation, characterization, and adsorption mechanism. Carbohydrate Polymers, 137, 402–409.
- Rosa, M. F., Medeiros, E. S., Malmonge, J. A., Gregorski, K. S., Wood, D. F., Mattoso, L. H. C., et al. (2010). Cellulose nanowhiskers from coconut husk fibers: Effect of preparation conditions on their thermal and morphological behavior. *Carbohydrate Polymers*, 81, 83–92.
- Ruan, C. Q., Stromme, M., & Lindh, J. (2018). Preparation of porous 2,3-dialdehyde cellulose beads crosslinked with chitosan and their application in adsorption of Congo red dye. Carbohydrate Polymers, 181, 200–207.
- Shao, M., Xiu, L., Zhang, H., Huang, J., & Gong, X. (2018). Chitosan/cellulose-based beads for the affinity purification of histidine-tagged proteins. *Preparative Biochemistry & Biotechnology*, 48, 352–360.
- Smith, G. S., & Snyder, R. L. (1979). F_N : A criterion for rating powder diffraction patterns and evaluating the reliability of powder-pattern indexing. *Journal of Applied Crystallography*, 12, 60–65.
- Suenaga, S., & Osada, M. (2018). Self-sustaining cellulose nanofiber hydrogel produced by hydrothermal gelation without additives. Acs Biomaterials Science & Engineering, 4, 1536–1545.
- Sun, J., Sun, X., Zhao, H., & Sun, R. (2004). Isolation and characterization of cellulose from sugarcane bagasse. *Polymer degradation and stability*, 84, 331–339.
- Supramaniam, J., Adnan, R., Kaus, N. H. M., & Bushra, R. (2018). Magnetic nanocellulose alginate hydrogel beads as potential drug delivery system. *International Journal of Biological Macromolecules*, 118, 640–648.
- Szymańska-Chargot, M., Cybulska, J., & Zdunek, A. (2011). Sensing the structural differences in cellulose from apple and bacterial cell wall materials by Raman and FTIR spectroscopy. Sensors, 11, 5543–5560.
- Trivedi, P., Saloranta-Simell, T., Maver, U., Gradisnik, L., Prabhakar, N., Smatt, J. H., et al. (2018). Chitosan-cellulose multifunctional hydrogel beads: Design, characterization and evaluation of cytocompatibility with breast adenocarcinoma and osteoblast cells. Bioengineering, 5, 3.
- Trygg, J., Fardim, P., Gericke, M., Makila, E., & Salonen, J. (2013). Physicochemical design of the morphology and ultrastructure of cellulose beads. *Carbohydrate Polymers*, 93, 291–299.

- Wada, M., Chanzy, H., Nishiyama, Y., & Langan, P. (2004). Cellulose III₁ crystal structure and hydrogen bonding by synchrotron X-ray and neutron fiber diffraction. *Macro-molecules*, 37, 8548–8555.
- Wang, J., Wei, L., Ma, Y., Li, K., Li, M., Yu, Y., et al. (2013). Collagen/cellulose hydrogel beads reconstituted from ionic liquid solution for Cu(II) adsorption. Carbohydrate Polymers, 98, 736–743.
- Xu, Q., Chen, C., Rosswurm, K., Yao, T., & Janaswamy, S. (2016). A facile route to prepare cellulose-based films. *Carbohydrate Polymers*, 149, 274–281.
- Yang, L., & Wang, T. (2018). Preparation of cellulosic drug-loaded hydrogel beads through electrostatic and host-guest interactions. *Journal of Applied Polymer Science*, 135, 46593.
- Zeng, B., Wang, X., & Byrne, N. (2020). Cellulose beads derived from waste textiles for drug delivery. *Polymers*, 12, 1621.
- Chang, D. Y., Zhang, N., Song, P., Hao, J. Y., Wan, Y., Yao, X. H., et al. (2018). Functionalized cellulose beads with three dimensional porous structure for rapid adsorption of active constituents from pyrola incarnata. *Carbohydrate Polymers*, 181, 560–569.
- Zhang, Y., Huo, M., Zhou, J., Zou, A., Li, W., Yao, C., et al. (2010). DDSolver: An add-in program for modeling and comparison of drug dissolution profiles. *The AAPS Journal*, 12, 263–271.
- Zhou, Y., Fu, S., Zhang, L., Zhan, H., & Levit, M. V. (2014). Use of carboxylated cellulose nanofibrils-filled magnetic chitosan hydrogel beads as adsorbents for Pb(II). Carbohydrate Polymers, 101, 75–82.